# Potent amyloidogenicity and pathogenicity of Aβ43

Takashi Saito[1#], Takahiro Suemoto[1#], Nathalie Brouwers[2,3], Kristel Sleegers[2,3], Satoru Funamoto[4], Naomi Mihira[1], Yukio Matsuba[1], Kazuyuki Yamada[4], Per Nilsson[1], Jiro Takano[1], Masaki Nishimura[6], Nobuhisa Iwata[1,7], Christine Van Broeckhoven[2,3] Yasuo Ihara[4], and Takaomi C. Saido[1*]

[1]Laboratory for Proteolytic Neuroscience, RIKEN Brain Science Institute, 2–1 Hirosawa, Wako-shi, Saitama 351–0198, Japan; [2]Neurodegenerative Brain Diseases Group, Department of Molecular Genetics, VIB, Antwerpen, Belgium; [3]Laboratory of Neurogenetics, Insititute Born-Bunge, University of Antwerp, Antwerpen, Belgium; [4]Faculty of Life Sciences, Doshisha University, Kyoto 619–0225, Japan; [5]Research Resource Center, RIKEN Brain Science Institute; [6]Molecular Neuroscience Research Center, Shiga University of Medical Science, Shiga 520–2192, Japan; [7]Department of Molecular Medicinal Sciences, Division of Biotechnology, Nagasaki University Graduate School of Biomedical Sciences, Nagasaki 852–8521, Japan.

[#]These authors contributed equally to this work.

*Correspondence should be addressed to T.C.S. (saido@brain.riken.jp)

**ABSTRACT**

**Aβ42 is known to be a primary amyloidogenic and pathogenic agent in Alzheimer's disease. However, the role of Aβ43, found just as frequently in patient brains, remains unresolved. We generated knockin mice containing a pathogenic presenilin-1 R278I mutation that causes overproduction of Aβ43. Homozygous mice exhibited embryonic lethality, indicating that the mutation involves loss of function. Crossing amyloid precursor protein transgenic mice with heterozygous mutant mice resulted in elevation of Aβ43 levels, impairment of short-term memory, and acceleration of Aβ pathology, accompanying pronounced accumulation of Aβ43 in plaque cores similar to the biochemical composition observed in patient brains. Consistently, Aβ43 showed a higher propensity to aggregate and was more neurotoxic than Aβ42. Other pathogenic presenilin mutations also caused overproduction of Aβ43 in a manner correlating with Aβ42 and with age of disease onset. These findings indicate that Aβ43, an overlooked species, is potently amyloidogenic, neurotoxic, and abundant in vivo.**

Alzheimer's disease, the most common form of dementia, is characterized by two pathological features in the brain, extracellular senile plaques and intracellular neurofibrillary tangles. Senile plaques consist of amyloid-β peptide (Aβ) generated from amyloid precursor protein (APP) through sequential proteolytic processing by β-secretase and γ-secretase. Two major forms of Aβ exist, Aβ40 and Aβ42, with Aβ42 being more neurotoxic due to its higher hydrophobicity, which results in faster oligomerization and aggregation[1]. A number of mutations associated with early-onset familial Alzheimer's disease (FAD) have been identified in the *APP*, *PSEN1* and *PSEN2* genes, and these mutations lead to accelerated production of Aβ42 or an increase in the Aβ42/Aβ40 ratio. Together these findings indicate that Aβ42 plays an essential role in the initiation of pathogenesis. However, the possible involvement of longer Aβ species that also exist in Alzheimer's disease brains has not yet been fully investigated.

Thus far, various longer Aβ species, such as Aβ43, Aβ45, Aβ48, Aβ49 and Aβ50, have been qualitatively described in Alzheimer's disease brains[2]. Similar Aβ species have also been found in transgenic mice that overexpress *APP* carrying FAD-linked mutations[3]. Further quantitative studies have revealed that Aβ43 is deposited more frequently than Aβ40 in both sporadic Alzheimer's disease (SAD) and FAD[4–7].

How these Aβ species with different C-terminal ends are generated from the precursor has mainly been investigated by cell biological and biochemical methods. A number of studies[8,9] demonstrated that γ/ε-cleavage by γ-secretase activity controls the fate of the C-terminal end. Aβ43, generated from Aβ49 via Aβ46, is subsequently converted to Aβ40 by γ-secretase whereas Aβ42 is independently generated from Aβ48 via Aβ45. It has also been reported that the FAD-associated I213T mutation in the *PSEN1* gene increases the generation of longer Aβ species, such as Aβ43, Aβ45 and

those even longer than Aβ46, in addition to Aβ42[10]. It is also noteworthy that Aβ43 appears to be equally as prone to aggregate *in vitro* as Aβ42[11], leading to faster formation of oligomers than occurs in the case of Aβ40[12]. These observations imply that Aβ43 could be produced as a physiological or pathological metabolite of γ-secretase activity and may affect Aβ amyloidosis in the brain.

In order to address whether Aβ43 contributes to Alzheimer's disease pathology, we decided to take advantage of the molecular phenotype of the presenilin-1 (PS1)-R278I mutation, as this mutation results in selective overt production of Aβ43 *in vitro*[13], an effect which occurs to a much greater extent than in the case of other mutations such as R278K, R278S and R278T. The R278I mutation had independently been reported in a pedigree suffering from atypical Alzheimer's disease with language impairment[14]. A follow-up survey revealed that one of the patients subsequently progressed to more severe cognitive impairment, and another patient from a different branch of the family with the mutation showed Alzheimer's disease-associated symptoms with an early loss of episodic memory and with a clinical onset of the disease at the age of 59 (Rossor M.N., personal communication).

In this study, we generated PS1-R278I knockin mice to assess the biological significance of the mutation and the pathological effect of Aβ43 on Aβ amyloidosis. Surprisingly, homozygous knockin mice showed embryonic lethality, presumably due to a partial loss of γ-secretase activity resulting in a failure in Notch1 processing. Consistent with this, mouse embryonic fibroblasts (MEFs) derived from the homozygous knockin mice exhibited a failure in PS1 endoproteolysis and Notch1 processing, implying that the particular selectivity of the PS1-R278I mutation for Aβ43 production is closely associated with the partial loss of γ-secretase activity, *i.e.*

suppression of the Aβ43-to-Aβ40 conversion, which could also be caused by some of the other PS1 mutations. We then demonstrated that heterozygous knockin mice crossbred with APP transgenic (Tg) mice exhibit short-term memory loss prior to plaque formation and develop considerably accelerated amyloid pathology, establishing that Aβ43 is potently amyloidogenic and pathogenic *in vivo*.

## RESULTS

### Generation of PS1-R278I knockin mice

To generate PS1 knockin mice, we constructed a targeting vector carrying a point mutation that results in amino-acid replacement of R278I in exon 8 of the *PSEN1* allele (**Supplementary Fig. 1a**). Homologous recombination, germline transmission and genotype were confirmed by Southern blotting and PCR (**Supplementary Fig. 1b,c**). The expression levels of the mutant and wild-type PS1 in the embryonic mouse brains were identical (**Supplementary Fig. 1d**). Unexpectedly, homozygous knockin (R278I/R278I) mice exhibited embryonic lethality at E15–18 (**Fig. 1a**). The mutant embryos showed an overall size reduction, a stubby tail, limb ateliosis and hemorrhage in the central nervous system (CNS) as compared to wild-type (+/+) littermate controls (**Fig. 1a**).

This phenotype is similar to that of PS1-deficient mice and Notch1-related mutant mice[15,16], although the adverse phenotype of the PS1-R278I knockin animals appeared a few days later than that of PS1-deficient mice. In contrast, we observed no developmental deficits in heterozygous knockin (+/R278I) mice (**Fig. 1a and Supplementary Fig. 2**). The lethal phenotype of the R278I mutation appears to be caused by a loss of developmental function that manifests only under the recessive condition. In addition, we generated two lines of double mutant mice: R278I knockin/PS1 knockout and M146V knockin/PS1 knockout. The former was embryonic lethal, the latter normal (**Supplementary Fig. 3a–d**). This observation suggests the characteristic loss-of-function nature of the R278 mutation. To our knowledge, this is the first case of developmental abnormality caused by a FAD-linked PS1 point mutation.

**Abnormal PS1 endoproteolysis and Notch1 processing**

In order to assess the functional significance of the R278I mutation in the PS1 knockin line, we analyzed the biochemical properties of PS1-R278I γ-secretase in the embryonic brains prior to degeneration (**Fig. 1a**). Western blotting revealed a dramatic decrease in the levels of the N-terminal fragment (NTF) and C-terminal fragment (CTF) of PS1, indicating a failure of PS1 endoproteolysis, in the homozygous knockin brains, whereas the γ-secretase components, including Nicastrin (Nct), presenilin enhancer-2 (Pen-2) and anterior pharynx defective-1 protein (Aph-1), were expressed at normal levels (**Fig. 1b**). The NTF and CTF in the homozygous knockin mice were, however, clearly detectable, indicating that a fraction of the endoproteolytic activity of PS1 still remained (**Fig. 1b and Supplementary Fig. 3e**). It is also noteworthy that the endoproteolysis was partially blocked in the heterozygous PS1-R278I brain, suggesting that the process is at least in part autolytic.

We next investigated whether the PS1-R278I mutation affects the assembly of the γ-secretase complex by Blue Native PAGE (BN-PAGE)[17]. A major signal corresponding to a molecular weight of 360 kDa, the normal molecular weight of the native PS1 γ-secretase complex, was detected in both the wild-type and knockin brains in a manner similar to that of the PS2 γ-secretase complex (**Fig. 1c**). Immunoprecipitation experiments further demonstrated that the mutant PS1 formed a complex with Nct, Pen-2 and Aph-1 (**Fig. 1d**). These data indicate that the PS1-R278I mutation does not affect the formation of the γ-secretase complex. Interestingly, BN-PAGE detected a minor signal corresponding to a higher molecular weight of 750 kDa in the homozygous knockin brains (**Fig. 1c: arrowhead**). A similar higher

molecular weight signal has previously been described in preparations from a patient with a deletion of exon 9 in the *PSEN1* gene (PS1-ΔE9)[17] and from SH-SY5Y cells treated with a γ-secretase inhibitor, L-685,458[18]. PS1-ΔE9 and PS1-ΔT440 also cause PS1 endoproteolytic abnormality in a similar manner to the PS1-R278I mutation[19–21]. The presence of this high molecular weight γ-secretase may reflect a conformational change in the multi-component complex or binding of additional factor(s) to the complex, although its mechanistic involvement remains unclear.

We then examined the effect of the mutation on the metabolism of the γ-secretase substrates. Both the CTF-α and CTF-β of APP and the CTF of N-cadherin accumulated at significant levels in the homozygous PS1-R278I knockin mouse brain but not in the wild-type or heterozygous brains (**Fig. 1e**). Conversely, APP intracellular domain (AICD) and Notch1 intracellular domain (NICD) could not be detected in the homozygous knockin. An additional signal smaller than that of CTF-α appeared in the knockin mice (**Fig. 1e: asterisk**), presumably representing an aberrant proteolytic product of CTF-α and β. These data indicate that the PS1-R278I mutation leads to a significant loss of γ-secretase activity in a recessive manner.

In order to further analyze the mutant γ-secretase, we established MEFs from knockin mice and littermate controls. Western blotting (**Supplementary Fig. 4a**), BN-PAGE (**Supplementary Fig. 4b**) and Immunoprecipitation experiments (**Supplementary Fig. 4c**) demonstrated that the biochemical properties of mutant PS in MEFs were identical to those in the embryonic brains. We then expressed Myc-tagged ΔNotch1 in the mutant and wild-type MEFs. Western blot analysis revealed that conversion of Myc-ΔNotch1 to Myc-NICD by limited proteolysis takes place in wild-type and heterozygous knockin MEFs but not in the homozygous knockin or PS1

knockout MEFs (**Fig. 1f**). These results indicate that the R287I mutation induces developmental deficits by abolishing of γ-secretase-dependent Notch1 processing.

**Aβ40, Aβ42 and Aβ43 in PS1-R278I knockin brains and MEFs**

Because homozygous R278I knockin mice are embryonic lethal, we went on to analyze adult heterozygous knockin mice. The adult heterozygous mice at 3 and 24 months of age were normal in development and anatomy (**Supplementary Fig. 2**), whereas various biochemical properties of PS1, such as partial abnormality of endoproteolysis, the molecular weight of γ-secretase and the identity of the complex components, were identical to those of the heterozygous embryonic brain (**Supplementary Fig. 5**). We then established a specific and highly sensitive ELISA systems that could distinguish between Aβ40, Aβ42 and Aβ43 over a broad concentration range (**Fig. 2a,b and Supplementary Figs. 6a,b and 7**). The antibodies used were highly specific to each Aβ species (**Fig. 2c–e and Supplementary Fig. 6c–e**). Brain tissue fractions soluble in Tris-HCl buffered saline (TS) and those that could be dissolved in 6M guanidine-HCl (GuHCl) were subjected to quantification.

There was a significant decrease in the steady state levels of GuHCl-Aβ40 in the brains of aged (24-months-old) heterozygous PS1-R278I knockin mice as compared to wild-type animals, although no differences were recorded in the levels of TS-Aβs, GuHCl-Aβ42 and GuHCl-Aβ43 (**Fig. 2f,g**). This reduction of GuHCl-Aβ40 resulted in a significant elevation of the Aβ42/Aβ40 and Aβ43/Aβ40 ratios in the GuHCl-soluble fraction (**Fig. 2h,i**). Notably, the Aβ43/Aβ42 ratio was also significantly increased in the GuHCl-soluble fraction of the heterozygous PS1-R278I knockin mouse brain (**Fig. 2j**). In younger PS1-R278I knockin mice (3 months old), Aβ43 levels were too low to

detect, although the GuHCl-Aβ40 levels were again significantly reduced in the knockin mice (**Supplementary Fig. 8**). These results indicate that Aβ43 levels in the mouse brain increase upon aging, and that the increase in the Aβ42/Aβ40 and Aβ43/Aβ40 ratios observed in the older heterozygous mice appears to be primarily caused by a decrease in Aβ40. Furthermore, the R278I mutation leads to an elevation in the Aβ43/Aβ42 ratio in aged mice. Taken together, these findings indicate that the PS1-R278I mutation gave rise to a modest *in vivo* effect in terms of the levels of endogenous Aβ species under heterozygous conditions.

We next quantified the Aβ variants in conditioned medium from knockin MEFs (**Fig. 2k–n**). The steady state levels of Aβ40 were significantly reduced in a gene-dose-dependent manner in the PS1-R278I MEFs as compared to wild-type MEFs. In contrast, Aβ43 markedly increased in the homozygous knockin MEFs, whereas Aβ42 levels remained unchanged in all genotypes (**Fig. 2k**). Thus, the ratios of longer Aβ species significantly increased in homozygous PS1-R278I knockin MEFs (**Fig. 2l–n**). Intriguingly, there was no increase in Aβ43 levels in conditioned media from heterozygous knockin MEFs (**Fig. 2k**). To unravel the underlying mechanism, we generated heterozygous R278I knockin x PS1 knockout mice (R278I/–) and measured the levels of Aβs in conditioned media from cultured MEFs. Indeed Aβ43 levels were increased, implying that, in heterozygous PS1-R278I knockin MEFs, wild type PS1 process Aβ43 to Aβ40 (**Fig. 2k**). Furthermore, in heterozygous PS1 knockout, no Aβ43 could be detected (data not shown). Together, the data suggests that the γ-secretase substrate can be transferred between separate PS1 molecules or between dimmers of PS1 as previously suggested[22] or even between PS1 molecules within the PS1 complexes, for further processing. The fact that total Aβ (Aβ40 + Aβ42 + Aβ43) was

decreased in heterozygous knockin MEFs, compared to homozygous knockin MEFs, is of particular interest. It might be due to a dysfunctional PS1 heterodimer where wild type PS1 is either directly affected by PS1-R278I or overloaded with Aβ43 generated by PS1-R278I. Further experiments are required to resolve the reason behind the decreased total Aβ level (**Fig. 2k and Supplementary Fig. 9b**). Taken together, the R278I mutation inhibits Aβ43 to Aβ40 conversion leading to increased Aβ43 levels and concomitant decrease of Aβ40, without altering Aβ42 levels. A similar Aβ-processing pathway has been previously described by Takami et al[9] (**Fig. 2k and Supplementary Fig. 10**).

**Aβ pathology and memory impairment of APP Tg mice**

Overexpression of wild-type human APP (hAPPwt) in the above-stated MEFs using a semliki-forest virus vector[23] resulted in a significant increase in Aβ43 in the heterozygous R278I knockin cells (**Supplementary Fig. 9**). The presence of the excessive γ-secretase substrates, *i.e.* APP CTF-α and β, appears to have forced the mutant PS1 to participate in APP processing. These observations prompted us to crossbreed heterozygous PS1-R278I knockin mice with APP Tg mice (APP23) to assess the effect of Aβ43 *in vivo*. APP Tg x PS1-R278I knockin mice started to accumulate pathological Aβ deposits at around 6 months of age, whereas it took about 12 months for single APP-Tg mice to begin to show signs of such deposition (**Fig. 3a–d,g,h**). Massive astrocytosis was also detected around the amyloid plaques already at 9 months age in the APP Tg x PS1-R278I knockin mice but not in single Tg mice (**Fig. 3e,f**). Behaviorally, 3–4 month old APP Tg x PS1-R278I knockin mice exhibited short-term memory impairment as compared to single Tg mice when their performance was tested

in a Y-maze test (**Fig. 3i,j**). A similar tendency was also observed in the Morris water maze test, although the difference in this case did not reach statistic significance (**data not shown**). Taken together, the above findings indicate that the PS1-R278I mutation leads to accelerated Aβ pathology with an accompanying inflammatory response, and that the significant cognitive impairment occurs even prior to plaque formation.

We next quantified the steady state levels of Aβ40, Aβ42 and Aβ43 in the brains of APP Tg and APP Tg x PS1-R278I knockin mice at 3 and 9 months. Notably, only the double mutant mice exhibited selective elevation of Aβ43 in both TS-soluble and GuHCl-extractable brain fractions at 3 months, prior to the pathological deposition of Aβ (**Fig. 4a–f**), but at a time-point when the double mutant mice already showed short-term memory impairment (**Fig. 3i,j**). In contrast, Aβ40 and Aβ42 levels started to increase at around 9 months. Consequently, both the Aβ43/Aβ40 and Aβ43/Aβ42 ratios were higher in the double-mutant mice than in the single APP Tg mice at both 3 and 9 months, whereas the Aβ42/Aβ40 ratio remained unaltered (**Fig. 4g–i**). It is worth noting that the elevation of biochemically detectable Aβ43 levels preceded plaque formation, implying that Aβ43 may be the initial seeding species and the trigger of memory impairment in this mouse model. The steady state level of Aβ43 also increased in an age-dependent manner in the single APP Tg mouse brains, beginning prior to the plaque formation (**Fig. 3g,h and Supplementary Fig. 11**).

In addition, we observed that a variety of FAD-associated PS1 mutations resulted in overproduction of Aβ43 in a manner correlating with the quantity of Aβ42 as well as with the age of onset of the patients[24] (**Fig. 5** and **Supplementary Fig. 12**). These observations indicate the presence of an intrinsic mechanism by which Aβ43 is physiologically generated and that not only Aβ42 but also Aβ43 may be involved in

Alzheimer's disease pathogenesis. The reason for the correlation between Aβ42 and Aβ43 remains elusive.

**APP Tg x PS1-R278I versus APP Tg x PS1-M146V knockin mice**

We also made another line of double-mutant mice by crossbreeding the APP Tg mice with PS1-M146V knockin mice as a positive control with which to compare the APP Tg x PS1-R278I knockin mice, given that the former mutation results in overproduction of Aβ42 rather than Aβ43[25] As expected, the PS1-M146V mutation, unlike the PS1-R278I mutation, resulted in selective accumulation of Aβ42 (**Supplementary Fig. 13**). Although the steady state levels of Aβ42 in the APP Tg x PS1-M146V mice was about 10-fold greater than that of Aβ43 in APP-Tg x PS1-R287I mice at 9 months, the total plaque areas, as determined by immunohistochemistry, were similar (**Fig. 6**). Both double-mutant lines accumulated Aβ40 and Aβ42, whereas Aβ43 occurred much more abundantly in the APP Tg x PS1-R278I mice (**Fig. 6a,b**). Quantitative image analyses gave consistent results (**Fig. 6c–e**). Aβ43 immunoreactivity colocalized with the plaque cores in a manner similar to that of Aβ42 but not Aβ40 (**Fig. 6f–h**). Interestingly, Aβ species with the 3rd N-terminal residue converted to pyroglutamate (N3pE-Aβ), a potently pathogenic Aβ subspecies[26–29], also colocalized with plaque cores and deposited more abundantly in APP Tg x PS1-R278I mice than in APP Tg x PS1-M146V animals (**Supplementary Fig. 14**). Although the underlying mechanism that accounts for the elevated N3pE-Aβ generation in the APP Tg x PS1-R278I mice remains unclear, the observation is consistent with a previous report that some presenilin mutations increase the quantity of N-terminally truncated Aβ in the brains of FAD patients[30].

Although APP Tg x PS1-M146V mice accumulated greater numbers of Aβ

plaques in the cortical and hippocampal areas than APP Tg x PS1-R278I mice, the density of thioflavin S-positive plaques per total plaques was significantly greater in the APP Tg x PS1-R278I knockin mice (**Fig. 7a–f**). This observation indicates that Aβ43 is even more prone to seed cores in plaque formation than Aβ42. To test this hypothesis *in vitro*, we performed thioflavin T binding experiments using an equal amount of Aβ40, Aβ42 and Aβ43 (20 μM each). Aβ43 induced the highest incorporation of thioflavin T into Aβ aggregates (**Fig. 7g**). In addition, stoichiometric experiments, in which we added a relatively small quantity of Aβ40, Aβ42 or Aβ43 (0.2 μM) to a mixture of Aβ40 (20 μM) and Aβ42 (2 μM), also showed that Aβ43 most potently accelerated incorporation of thioflavin T (**Fig. 7h**). These indicate that Aβ43 contributes to the formation of the thioflavin T-positive β-sheeted structure to a greater extent than either Aβ40 or Aβ42, a finding that may account for the observation that a relatively small amount of Aβ43 is sufficient to accelerate Aβ amyloidosis and induce plaque core formation *in vivo*.

**Neural toxicity and amyloid pathology of Aβ43**

In agreement with Aβ42 having higher hydrophobicity and higher toxicity than Aβ40 *in vitro* and *in vivo*, a large number of reports also show that Aβ42 contributes to synaptic dysfunctions[31–34]. Herein, we compared the toxicity of Aβ40, Aβ42 and Aβ43. Aβ43 and showed a higher potent neural toxicity in a dose-dependent manner as compared to Aβ40 and Aβ42 (**Fig. 7i,j**). These results anticipate that Aβ43 directly affects neural toxicity and induces synaptic dysfunction, which would contribute to short-term memory impairments prior to the amyloidogenesis (**Fig. 3i.j**).

Finally, we performed immunohistochemical experiments on brain sections from SAD patients to explore the possible involvement and significance of Aβ43 in human neuropathology. Aβ43 accumulated in the brains more frequently than Aβ40 (**Fig. 8a–e and Supplementary Fig. 15**), and was present in both diffuse (**Fig. 8f,g**) and dense-cored (**Fig. 8h,i**) plaques, similar to Aβ42 and N3pE-Aβ (**Supplementary Fig. 16a–d**). Furthermore, thioflavin S fluorescence signals colocalized well with Aβ43 immunoreactivity (**Fig. 8j–m**), as well as with N3pE-Aβ (**Supplementary Fig. 16e–g**). These observations are consistent with those of previous studies showing that a substantial amount of Aβ43 accumulates in SAD and FAD brains[4–7].

## DISCUSSION

Previous studies have elegantly demonstrated that Aβ42 is essential for amyloid deposition *in vivo*[31] and that Aβ40 inhibits this deposition[32], based on the use of Bri-Aβ fusion proteins. The difference between Aβ40 and Aβ42 lies in the carboxyl-terminal amino-acid sequence, *i.e*. the additional presence of isoleucine and alanine residues in Aβ42. Because both isoleucine and alanine are hydrophobic amino acids, it is reasonable to assume that Aβ42 is more prone to form a β-sheet structure than Aβ40. In contrast, the carboxyl-terminal amino acid of Aβ43 is threonine, which carries a hydrophilic alcohol group (together with a hydrophobic methyl group) and thus could reverse the hydrophobicity of Aβ42. Therefore, the amyloidogenicity of Aβ43, a natural product of γ-secretase activity[8,9], has remained elusive.

Herein, we focused on Aβ43, an overlooked species in AD research, to investigate a crucial role in amyloidogenesis and pathogenesis of AD. So far, the major focus has been placed on the amyloidogenecity of Aβ42 and in numerous studies; BC05, an anti-Aβ42 antibody has been used to demonstrate that Aβ42 is the major pathogenic species in AD. Since partial crossreactivity of BC05 against to Aβ43 had already been reported[47], Aβ42(43), like this orthography, was noted in some of the carefully designed and interpreted studies using BC05, as a tacit understanding. However, many of other studies apparently overestimated the Aβ42 levels and ignored the possible changes in Aβ43 levels. Almost all FAD-associated PS1 mutations result in an increase of the Aβ42/Aβ40 ratio caused by an increase of Aβ42 levels. However, some of the PS1 mutations lead to a decrease of Aβ40 with or without alteration of Aβ42 levels which also leads to an increase of the Aβ42/Aβ40 ratio. One explanation of the association between decreased Aβ40 and FAD could possibly be that Aβ40 plays a role in

protection from plaque fromation[32]. We here report that in PS1-R278I knockin mice, Aβ40 levels are decreased accompanying increased levels of Aβ43. Furthermore, the increased Aβ43 levels accelerated Aβ pathology, thus contributing to the early onset of the disease. Therefore, we propose that Aβ43 be separately analyzed apart from Aβ42.

In an effort to explore the role of Aβ43 in Aβ amyloidosis, we generated PS1-R278I knockin mice based on the knowledge that this mutation causes overproduction of Aβ43 *in vitro*[13]. We chose to use this PS mutation knockin paradigm rather than the overexpression strategy for the following reasons. First, the R278I mutation is known to be clinically pathogenic. The knockin paradigm is also less artificial than Tg overexpression approaches in general, and we considered that the knockin mice could potentially be utilized to generate a relevant AD model by crossbreeding with other mice such as mutant APP Tg or knockin mice. Unexpectedly, the phenotype of the homozygous knockin mice proved to be embryonic lethal in association with abnormal PS1 endoproteolysis. Limited proteolysis of APP CTF-α, CTF-β, N-cadherin and Notch1 was also hampered in the homozygous knockin embryos, although the γ-secretase components appeared to have been properly assembled to a 360 kDa complex. Based on previous studies, it appears that the disturbance in Notch1 processing represents the primary cause of the premature death that we observed[16,35]. Compared to PS1 knockout, the embryonic lethality of PS1-R278I knockin mice occurs at a slightly later stage. Taking into account that a 50 % reduction of γ-secretase activity in heterozygous PS1-R278I or in heterozygous PS1 knockout does not lead to embryonic lethality while the 90% reduction in homozygous PS1-R278I does so, it seems that the γ-secretase activity threshold for survival is

somewhere between 10–50 % of wild type. The remaining 10% γ-secretase activity in homozygous PS1-R278I knockin could account for the delayed lethality compared to PS1 knockout (**Supplementary Fig. 10c**). Taken together, these results strongly suggested that the primary phenotype of the R278I mutation was a partial loss of function in terms of γ-secretase activity.

Despite this, MEFs prepared from homozygous embryos produced an extremely large steady state levels of Aβ43 (approximately 20-fold greater than that of wild-type MEFs); this accompanied a significant decrease in Aβ40 production and no changes in Aβ42 levels. Previous *in vitro* studies have also demonstrated that Aβ43 is processed to Aβ40 whereas Aβ42 is independently produced from Aβ45 in the presence of γ-secretase[8,9]. In agreement with these studies, our results from crossbreeding heterozygous PS1-R278I mice with PS1 knockout mice, which showed significant levels of both Aβ40 and Aβ43, indicated that Aβ43 was indeed converted to Aβ40 independently of Aβ42 production (**Fig. 2k**). Furthermore, we found that the ratio of production of Aβ46 in homozygous PS1-R278I MEFs was increased with a concomitant increase of Aβ43 and decrease of Aβ40 in *in vitro* γ-secretase assays (**Supplementary Fig. 10**), suggesting that production of Aβ40 and Aβ43 also depends on Aβ46 production as previously postulated[8–10]. Thus, inhibition of this Aβ43-to-Aβ40 conversion could account for the increase in Aβ43 and the concomitant decrease in Aβ40 in the knockin MEFs. Interestingly, treatment of PS1-ΔE9-expressing cells with L-685,458 resulted in elevated Aβ43 production[36], consistent with the notion that multiple processes are involved in the generation of various Aβ species and that a partial loss of γ-secretase activity might give rise to a particular Aβ species. However, *in vitro* γ-secretase activity of heterozygous and homozygous PS1-R278I was drastically

reduced in a gene-dose-dependent manner, while there were no significant differences of the steady state levels of total MEF-produced Aβ compared to wild type MEFs. To elucidate the reason behind this contradiction, it will be necessary to investigate other mechanisms *e.g.* intracellular trafficking and secretion of Aβ in depth.

The molecular mechanism that allows Aβ43 production but not other proteolytic processes remains to be clarified, but it is likely to involve specific conformational changes of the γ-secretase complex[37]. Because Aβ42 is produced independently of Aβ43 in the presence of γ-secretase, some of the FAD-associated PS1 mutations that cause a decrease in Aβ40 without an increase in Aβ42, such as A79V, A231V, C263F, L282V, L166P and G384A[24,38], might actually result in the elevation of Aβ43 in a manner similar to the R278I mutation. In addition, PS1-ΔE10, an artificial PS1 mutation located to the loop domain of PS1 where R278I is present, showed a significant reduction of the steady state levels of Aβ40 without any alteration of the Aβ42 levels similar to our results, however Aβ43 levels were not measured[39]. It will therefore be important to investigate if these FAD-associated mutations give rise to increased Aβ43 levels and importantly, scrutinize their amyloidogenicity. In fact, I143T, L262F, L282V and G384A mutations did lead to significant production of Aβ43 in our transfection assays. Notably, Aβ43 levels and the ratio of Aβ43/Aβ40 significantly correlated well with the age of disease onset in a manner similar to Aβ42 levels and the ratio of Aβ42/Aβ40. Additionally, a PS1-I143T carrier in a Swedish family with FAD gave rise to high levels of Aβ43[7]. These observations highlighted the possibility that compounds that facilitate the Aβ43-to-Aβ40 and Aβ42-to-Aβ38 conversion might be beneficial for prevention and treatment of AD by decreasing not only Aβ42 but also Aβ43. In support of this notion, an oral vaccination with adeno-associated virus vector

carrying Aβ1−43 cDNA was reported to result in a marked reduction of Aβ burdens and improvement of behavioral performances in APP transgenic mice[40,41].

Although our original plan had been to establish APP Tg x homozygous PS1-R278I knockin mice, we also explored the possible utility of heterozygous PS1-R278I knockin mice, given that overexpression of APP in heterozygous PS1-R278I knockin MEFs resulted in selective elevation of Aβ43. Consistent with this, APP Tg x heterozygous PS1-R278I knockin mice exhibited short-term memory impairment, selective biochemical accumulation of Aβ43 at an early stage prior to plaque formation and significant acceleration of Aβ pathology thereafter as compared to single APP Tg mice. It is also important to note that the APP Tg x PS1-R278I knockin mice exhibited a greater density of the thioflavin S-positive signal per plaque than APP Tg x PS1-M146V knockin mice, which overproduce Aβ42 instead of Aβ43. Consistent with previous reports[6,7], we have observed Aβ43-positive plaques more often than Aβ40-positive ones in AD brains. Aβ43 has previously been found in amyloid plaques not only in AD patients[4,6,7] but also in aged gorillas[42] and in some AD model mice harboring PS1 or APP FAD-mutations[3,10]. In addition, it has been suggested that the amount of Aβ43 in plaques correlates with cognitive decline[5]. We also showed in this report that Aβ43 exhibited potent neural toxicity, comparable to or even greater than that of Aβ42. These observations establish that Aβ43 is indeed amyloidogenic *in vivo* and likely to be pathogenic. Thus, the carboxyl-terminal amino acid residue of Aβ43, *i.e.* threonine, appears to strengthen the hydrophobicity of the peptide rather than reversing it.

Notably, biochemical accumulation of Aβ43 preceded pathological deposition in the APP Tg x PS1-R278I knockin mice and in the single APP Tg mice. In addition, the basal Aβ43 levels substantially increased with aging in wild-type mice up to at least

18 months of age (data not shown). These observations point to the possible value of Aβ43 as a biomarker for presymptomatic diagnosis of AD. We therefore believe that it would be worth trying to quantify Aβ43 levels in cerebrospinal fluid from AD patients and controls although this is beyond the scope of the present study. We also detected the presence of N3pE-Aβ in APP Tg x PS1-R278I knockin mouse brains, a finding that is supported by a report quantitatively describing N3pE-Aβ42 and N3pE-Aβ43 in the brains of FAD and SAD patients[2]. It is of particular interest that Pittsburgh Compound B, a probe for amyloid imaging by positron emission tomography, selectively binds to N3pE-Aβ[26], implying that N3pE-Aβ42/43 could be particularly prone to seed deposition of other Aβ species, consistent with previous reports[28]. It is also possible that the mutation might affect the interaction of PS1 with other substrates or alter its property of non-γ-secretase activity[29].

In summary, our observations establish that Aβ43, which has to large extent been overlooked, is potently amyloidogenic and toxic and highlight the potential value of Aβ43, i.e. CSF Aβ43 levels, as an early marker for some of the detrimental effects of aging in the adult brain. We propose that inhibition of Aβ43 generation, for instance, by facilitating the conversion of Aβ43 to Aβ40 in the γ-secretase complex should be beneficial for prevention of Aβ amyloidosis.

**Acknowledgments**

We thank M. N. Rossor (University College London, London, UK) for sharing clinical information about the R278I mutation carriers, J. Q. Trojanowski and V. M.-Y. Lee (University of Pennsylvania, Philadelphia, PA) for providing postmortem brain tissues, R. Kopan (Washington University, St. Louis, MO) for providing Myc-tagged ΔNotch1 plasmid, A. Takashima (RIKEN Brain Science Institute) for providing anti-Aph-1 antibody and J Hardy (University College London) for valuable discussions. This work was supported by research grants from RIKEN BSI, the Ministry of Education, Culture, Sports, Science and Technology, Ministry of Health, Labor and Welfare of Japan and TAKEDA Science Foundation, and the Fund for Scientific Research – Flanders (FWO-V), the Interuniversity Attraction Poles (IAP) program P6/43 of the Belgian Federal Science Policy Office and and a Methusalem Excellence Grant of the Flemish Government to C.V.B. N.B receives a FWO-V postdoctoral fellowship of the FWO-V.

**Author Contributions**

This study was jointly designed by T. Saito, T. Suemoto and T.C.S.; experiments were performed by T. Saito, T. Suemoto, N.M., Y.M., K.Y. and S.F.; and T. Saito, T. Suemoto, S.F., K.Y., P.N., J.T., M.N., N.I., C.V.B., Y.I. and T.C.S. jointly analyzed and interpreted data. N.B., K.S. and C.V.B. identified pathogenic PS1 mutations in patients/families and generated *PSEN1* vector constructs for expression studies.

**Figure Legends**

**Figure 1. Phenotypic and biochemical characterization of PS1-R278I knockin mice.**

(**a**) Embryonic lethality of homozygous PS1-R278I knockin mice. An overall size reduction, stubby tail (arrowheads), limb ateliosis (yellow arrows) and hemorrhage in the CNS (arrows) were observed. Scale bars: 2 mm. (**b**–**e**) Embryonic brains and (**f**) MEFs were subjected to Western blot analyses (see **Supplementary Fig. 4** for more information). Antibodies used are listed on the left side of each panel. (**b**) Expression of γ-secretase components. FL: full-length PS1. (**c**) BN-PAGE analysis of native γ-secretase complexes. The symbol (**–**/**–**) is used for the homozygous PS1 knockout mice used as a negative control. Arrows indicate the position of the native wild-type 360 kDa PS1 and PS2 γ-secretase complexes, whereas arrowheads point to the atypical high molecular weight (750 kDa) γ-secretase complex. (**d**) Immunoprecipitation by antibodies to PS1-NTF. IgG(H) and IgG(L) indicate immunoglobulin heavy and light chains, respectively. (**e**) γ-secretase activity in PS1-R278I knockin brains. Brain extracts were analyzed by Western blotting to detect endogenous APP-CTF-β, APP-CTF-α, AICD, full-length N-cadherin, N-cadherin-CTF and NICD products. (**f**) Notch1-processing in PS1-R278I knockin MEFs. Myc-tagged ΔNotch was transiently expressed in the MEFs, and cell lysates were subjected to Western blot analysis using anti-Myc antibody. β-actin levels are shown as internal controls.

**Figure 2. Aβ levels in adult PS1-R278I knockin mouse brains and MEFs.**

(**a,b**) Establishment of ELISA system to specifically quantify Aβ42 and Aβ43 (see more **Supplementary Figs 6a,b and 7**). (**c**–**e**) Specificity of the antibodies to Aβ40, Aβ42

and Aβ43 used in this ELISA system. Synthetic Aβ1−40, Aβ1−42 and Aβ1−43 were separated by Tris/Tricine PAGE (15% polyacrylamide gel) and subjected to Western blotting. Anti-Aβ antibodies, C40, C42 and C43, specifically recognized the Aβs, respectively (see more **Supplementary Fig. 6c−e)**. (**f−n**) Quantification of Aβ40, Aβ42 and Aβ43 by ELISA in adult mouse brains (**f−j**) and MEFs (**k−n**). (**f−j**) Cortical hemispheres from 24 month old wild-type and heterozygous knockin mice were homogenized and fractionated into TS-soluble and GuHCl-soluble fractions. Data represent mean ± s.e.m. ($n$ = 9). *$P$ < 0.05 and **$P$ < 0.01 between wild type and heterozygous knockin mice; Student-t test. (**k−n**) Aβ concentrations in conditioned medium from MEFs. $8x10^5$ cells were inoculated in a 1 ml culture. The conditioned medium was collected after 24 hrs and subjected to ELISA. The symbol (R278I/−) is used for the double heterozygote of PS1-R278I knockin crossbred with PS1 knockout mice. Data represent mean ± s.d. from two independent experiments ($n$ = 16). **$P$ < 0.01 compared with wild type; One-way ANOVA with Scheffe's F test.

**Figure 3. Acceleration of Aβ pathology and short-term memory impairment by the R278I knockin mutation in APP Tg mice.**

(**a−f**) Brain sections from APP Tg x PS1-R278I knockin mice (**a**: 3- , **b**: 6- , and **c, e**: 9-month old) and 9-month old single APP Tg mice (**d,f**) were immunostained with 4G8 anti-Aβ antibody (**a−d**) and anti-GFAP antibody (green) with 4G8 counterstaining (red) (**e,f**). Aβ immunostained brain sections from cortex (**g**) and hippocampus (**h**) of 3-, 6-, 9- and 12-month old wild-type, APP Tg, and heterozygous PS1-R278I knockin mice, as well as APP Tg x PS1-R278I knockin mice were analyzed ($n$ = 5−6 each genotype); *$P$ < 0.05 and **$P$ < 0.01 compared with APP Tg mice; Two-way ANOVA with Scheffe's F

test. Scale bars: 500 μm (**a–d**); 50 μm (**e,f**). (**i,j**) Y-maze test was performed prior to plaque formation using 3–4 month old male wild-type, PS1-R278I knockin, APP Tg and APP Tg x PS1-R278I knockin mice. Data represent mean ± s.e.m. ($n$ = 10 each genotype), *$P$ < 0.05 compared with wild type or PS1-R278I knockin mice; One-way ANOVA with Scheffe's F test.

**Figure 4 Aβ40, Aβ42 and Aβ43 in APP Tg x PS1-R278I knockin mice.**

(**a,d**) The levels of Aβ40, (**b,e**) Aβ42 and (**c,f**) Aβ43 were quantified by ELISA and (**g-i**) the ratios of the Aβ species were subsequently determined. Cortical hemispheres from single APP Tg and APP Tg x PS1-R278I knockin mouse brain (3 and 9 month old) were homogenized and fractionated into TS-soluble fractions (**a–c**) and GuHCl-extractable fractions (**d–f**). Data represent mean ± s.e.m. ($n$ = 7: 3 months old; $n$ = 5: 9 months old); *$P$ < 0.05 and **$P$ < 0.01 between APP Tg mice and APP Tg x PS1-R278I knockin mice; Student-t test.

**Figure 5. Effect of various pathogenic PS1 mutations on Aβ43 production.**

The constructs containing *PSEN1* with FAD-associated mutations were transfected into HEK293 cells stably expressing APP with the Swedish mutation: (**a**) Expression levels of PS1-FAD mutants. (**b–g**) Quantification of the steady state levels of Aβ40, Aβ42 and Aβ43 and the correlation between Aβ levels and the age of disease onset. Age of onset is shown as follows: wild type (75 years old), A79V (59.3), V94M (53), I143T (32.5), A231V (58), L262F (50.3), L282V (44) and G384A (34.9)[24,50]. Data represent mean ± s.d. from five independent series each consisting of duplicate measurements; *$P$ < 0.05 and **$P$ < 0.01 compared with wild type; One-way ANOVA with Dunnett test.

**Figure 6. Localization of Aβ species in amyloid plaques of APP Tg x PS1-R278I knockin mice.**

(**a**) A set of serial brain sections from 9 month old APP Tg x PS1-M146V knockin mice and (**b**) APP Tg x PS1-R278I knockin mice were immunostained with the following anti-Aβ antibodies as indicated: 4G8 (total Aβ), C40 (Aβx−40), C42 (Aβx−42) and C43 (Aβx−43). (**c−e**) The immunoreactive areas in single APP Tg (left column), APP Tg x PS1-M146V knockin (middle column) and APP Tg x PS1-R278I knockin (right column) mice were quantified as indicated ($n$ = 6); $^{**}P < 0.01$ between APP Tg x PS1-M146V knockin mice and APP Tg x PS1-R278I knockin mice; One-way ANOVA with Scheffe's F test. N.D.: not detected. (**f−h**) Double-staining with 4G8 (green) and the following Aβ species-specific antibodies (red): Aβ40 (**f**), Aβ42 (**g**) and Aβ43 (**h**). The images in the left (green) and middle (red) are merged (yellow) in panels on the right. Scale bars: 500 μm (**a,b**); 50 μm (**f−h**).

**Figure 7. Mature amyloid plaques in APP Tg x PS1-R278I knockin mice and *in vitro* aggregation property and neural cell toxicity of Aβ43.**

(**a−f**) A set of serial brain sections from 9 month old APP Tg x PS1-M146V knockin mice (**a,c**) and APP Tg x PS1-R278I knockin mice (**b,d**) were stained with thioflavin S (**a,b**) and immunostained with 4G8 (**c,d**). Thioflavin S positive plaque are marked with arrows (**a,b**) and the corresponding plaques in the serial brain sections are also marked (**c,d**), respectively. Scale bars: 500 μm (**a−d**). Intensity of cortical and hippocampal Aβ immunoreactivity and thioflavin S signals were quantified (**e**), and the ratio of thioflavin S/total Aβ signal of amyloid plaques was determined (**f**) ($n$ = 12); $^{**}P < 0.01$ between

APP Tg x PS1-M146V knockin mice and APP Tg x PS1-R278I knockin mice; Student-t test. (**g,h**) *In vitro* Aβ aggregation experiments. Incorporation of thioflavin T into Aβ aggregates was measured by fluorescence spectroscopy. (**g**) The aggregation property of 20 μM Aβ40, Aβ42 and Aβ43 at 20 μM was measured individually. (**h**) The effect of Aβ40, Aβ42 and Aβ43 at a concentration of 0.2 μM on the mixture of 20 μM Aβ40 and 2 μM Aβ42 was then assessed. Data represent mean ± s.d. from three independent series each consisting of 6–8 individual measurements; $^{**}P < 0.01$ (**g**) between Aβ40 and Aβ42 or between Aβ42 and Aβ43, $^{\#}P < 0.05$ (**h**) between Aβ40 and Aβ43; One-way ANOVA with Scheffe's F test. (**i,j**) Neural cell toxicity of Aβ43. Cell viability (i) and LDH release as a measure of cell toxicity (j) were assayed. Aβs were administrated at 1, 3 and 10 μM, respectively. The results obtained after treatment with Aβ40 (open column), Aβ42 (gray column) and Aβ43 (filled column) are indicated, and vehicle (veh) treatment was also indicated by open column in (**j**). Data represent mean ± s.d. from three independent series each consisting of 6 individual measurements; $^{*}P < 0.05$ and $^{**}P < 0.01$ between Aβ40 and Aβ42 or between Aβ42 and Aβ43, and $^{\#}P < 0.05$ between Aβ40 and Aβ43; Two-way ANOVA with Scheffe's F test or Dunnett test.

**Figure 8. Aβ43 in amyloid plaques in AD brains.**

(**a–d,f–i**) Serial sections of the hippocampal region (**a–d, h,i and j–m**) and the frontal cortical region of AD brains (**f,g**) were stained with the anti-Aβ antibodies 4G8 (total Aβ), C40 (Aβx–40), C42 (Aβx–42), and C43 (Aβx–43), as well as thioflavin S, as indicated. The single staining (**a–d,f–i**) was developed using 3,3'-diaminobenzidine, whereas the double-staining (**j–m**) utilized the fluorescent dyes fluorescein (green, Aβ) and rhodamine (red, Aβ43). The images in panels (**j**) and (**k**) are merged (yellow) in

panel (**l**). Scale bars: 250 μm (**a–d**); 25 μm (**f–m**). (**e**) Ratio of Aβ40, Aβ42 and Aβ43 of the plaque areas in the hippocampal region of AD brain sections from 4 individuals were quantified; $^{**}P < 0.01$ between Aβ40 and Aβ43; One-way ANOVA with Scheffe's F test (see **Supplementary Fig. 15** for more details).

## Methods

### Generation of PS1-R278I knockin mice

As shown in **Supplementary Fig. 1**, the genomic DNA of mouse *PSEN1* was isolated from the bacterial artificial chromosome (BAC) library from the 129/Sv mouse genome, and one BAC clone which included intron 5 to intron 11 of the *PSEN1* gene was obtained. The fragment from the ApaI site of intron 5 to the HindIII site of intron 11 provided the basis for construction of the targeting vector. To introduce the PS1-R278I mutation, the SmaI/BamHI fragment containing introns 7 and 8 of the *PSEN1* gene was subcloned into pBluescript vector. To introduce the R278I mutation the following primer was used (underlined: original G to T), 5'-GGTTGAAACAGCTCAGGAAA**T**AAATGAGACTCTCTTTCCAGC-3', using GeneEditor Mutagenesis System (Promega) according to the manufacturer's protocol. This fragment was used to replace the original sequence of the *PSEN1* gene. Finally, a *pgk-neo* gene cassette was inserted for positive selection at the EcoRI/SmaI sites located in intron 7, and a Diphtheria toxin-A fragment cassette was inserted for negative selection at the HindIII site in intron 11. We used the fragment of ApaI/EcoRI spanning from intron 5 to intron 7 (4.3kbp) as the long arm and the fragment of BamHI/HindIII spanning from intron 8 to intron 11 (3.8kbp) as the short arm of the targeting vector.

Embryonic stem (ES) cell cultures and gene-targeting experiments were carried out as previously described. Targeted ES cells were microinjected into 129/Sv blastocysts. DNA was extracted from the biopsied tail of mouse pups, and the F1 generation of the mutant animals was identified by Southern blot analysis with a 3' external probe which was produced by PCR using the following primer sets, 5'-AATGGATAATCAGAGCCTGCC-3' and

5’-TCCTCACAACTAACTACCCAAGG-3’.

The heterozygous mice were crossbred with EIIa-Cre transgenic mice to remove the *pgk-neo* gene, after which the generated PS1-R278I knockin mice were backcrossed to the C57BL6/J strain. When the *pgk-neo* gene was removed by the *cre-loxP* system, a short sequence ranging from the EcoRI to the SmaI sites of intron 7 was also removed. Deletion of such a short sequence in intron 7 leads to feasible detection of the genotype of mutant mice. To genotype the PS1-R278I knockin mouse, tail DNA was isolated and subjected to PCR analysis using the following primer sets: 5’-AGTTTCAGACCAGCCTAGGCCAC-3’ and 5’-AGGAAGGGAGACTTGACAGC-3’.

**Other mutant mice**

PS1 knockout mice and PS1-M146V knockin mice were purchased from the Jackson Laboratory. APP23 mice carrying the human APP695 transgene harboring the Swedish mutation (KM670/671NL)[43] have been described previously[44]. All animal experiments were carried out according to the RIKEN Brain Science Institute’s guidelines for animal experimentation.

**Mouse embryonic fibroblasts (MEFs)**

MEFs were prepared from E13–14 embryos of wild-type, PS1-R278I knockin and PS1 knockout mice, and inoculated in Dulbecco’s modified Eagle’s medium supplemented with 10% fetal bovine serum. The conditioned medium and cell lysates from MEFs (passage <8) were subjected to biochemical analyses, including ELISA, native-PAGE and Western blotting. Transfection of the MEFs with the Myc-tagged ΔNotch

construct[45] was performed using FuGENE 6 Transfection Reagent (Roche) according to the manufacturer's instructions.

**Blue native-polyacrylamide gel electrophoresis (BN-PAGE)**

Non-denaturing native PAGE was performed to confirm the integrity of the γ-secretase complexes[17] using the Novex Bis-Tris gel system (Invitrogen) according to the manufacturer's instructions. Samples were extracted from embryonic brains and MEFs using the sample buffer from the Novex Bis-Tris gel system that contains 1% digitonin. Equal amounts of proteins as determined using the BCA Protein Assay Kit (Pierce) were loaded on a 3–12% gradient Bis-Tris acrylamide gel. Immunoblotting was performed using H70 (anti-PS1 N-terminal antibody, Santa Cruz) and Ab-2 (anti-PS2 antibody, Calbiochem) antibodies.

**Immunoprecipitation assay and Western blot analysis**

Brain homogenates from embryonic brains (E14–16) and cell lysates of MEFs were immunoprecipitated with H70, and then captured by Dynabead conjugating protein G (Invitrogen). Immunoprecipitants were subjected to Western blot analysis using H70, MAB5232 (anti-PS1-Loop antibody, Chemicon), Ab-2, PA1-758 (anti-Nicastrin antibody, Affinity Bioreagents), anti-Pen-2 (Zymed), and ACS-01 (anti-Aph1 antibody)[10] antibodies. The following antibodies were also used in Western blot analysis: 6E10 (anti-Aβ1–12 antibody, Covance), 22C11 (anti-APP-N-terminal antibody, Chemicon), anti-APP-CTF antibody (Sigma), 9B11 (anti-Myc antibody, Cell Signaling), mN1A (anti-Notch1 antibody, BD Bioscience), and AC-15 (anti-β-actin antibody, Sigma).

**Enzyme-linked immunosorbent assay (ELISA)**

Soluble materials from mouse cortical hemispheres were dissolved in Tris-HCl buffered saline (TS fraction) and the insoluble materials were dissolved in guanidine-HCl solution (GuHCl fraction) as previously described[46]. Samples from the brains and from the conditioned medium of MEFs were analyzed using an Aβ-ELISA kit (Wako) to quantify Aβ40. In order to specifically quantify the levels of Aβ42 and Aβ43, we established an Aβ42- and Aβ43-specific sandwich ELISA system utilizing the Aβ-ELISA kit (Wako). Since BC05, a detection antibody of this kit, cross-reacts with Aβ42 and Aβ43 as previously described[47], we used the Aβ42- and Aβ43-specific antibodies, C42 (anti-Aβ42 specific antibody, IBL) and C43 (anti-Aβ43 specific antibody, IBL). The specificities of these antibodies are shown in **Fig.2c–e and Supplementary Fig. 6c–e**. Samples were incubated overnight at 4 ºC in a 96-well plate coated with the capture antibody, BNT77 (anti-Aβ11–28 antibody[48]). Aβ from samples captured in the ELISA were incubated with C42 or C43 (1:100, for 3 hr at room temperature), respectively, after which HRP-conjugated anti-rabbit IgG (1:500, for 2 hr at room temperature) was added as a detection antibody. Synthesized Aβ42 or Aβ43 peptide (Peptide Institute) was used for the preparation of a standard curve, and diluted with the diluents solutions provided in the kit. For consistency, when we quantified the amount of Aβ40, a synthesized Aβ40 peptide (Peptide Institute) was also used for the preparation of a standard curve. This system also worked in broader concentration range of Aβ42 and Aβ43 (**Supplementary Fig. 6a,b**). Furthermore, a high sensitive Aβ43 system, based on modified protocols, was established for the measurement of samples containing low amount of Aβ43, *e.g.* samples derived from non APP Tg mice and non

APP-overexpressing cells (**Supplementary Fig. 7**.)

**Immunohistochemical and histochemical studies**

Paraffin-embedded mouse brain sections were immunostained with the following antibodies: 4G8 (anti-Aβ17–24 antibody, Covance), C40 (anti-Aβ40 specific antibody, IBL). C42, C43 and MAB3402 (anti-GFAP antibody, Chemicon), with or without tyramide signal amplification (PerkinElmer Life Sciences) as previously described[46]. Quantification of immunoreactivity from brain sections were carried out using MetaMorph imaging software (Universal Imaging Corp.) as previously described[46].

**Y-maze test**

Mice were housed individually before transferring to the behavioral laboratory. They were kept during the behavioral analysis. The light condition was 12h:12h (lights on 8:00). The laboratory was air-conditioned and maintained temperature and humidity within approximately 22–23 ºC and 50–55%. Food and water were freely available except during experimentation. Large tweezers were used to handle mice in order to avoid individual differences in the handling procedure. All of the experiments were conducted in the light phase (9:00–18:00), and the starting time of the experiments was kept constant.

The Y-maze apparatus (O'Hara, Tokyo, Japan) was made of gray plastic, and consisted of three compartments (3 cm (W) bottom and 10 cm (W) top, 40 cm (L) and 12 cm (H)) radiating out from the center platform (3 x 3 x 3 cm triangle). The maze was positioned 80 cm above the floor, surrounded by a number of desks and test apparatuses around the maze to act as spatial cues. In this test, each mouse was placed in the center

of the maze facing towards one of the arms, and was then allowed to explore freely for 5 min. Experiments were performed at a light intensity of 150 lux at the platform. An arm entry was defined as four legs entering one of the arms, and the experimenter counted the sequence of entries by watching a TV monitor behind a partition. An alternation was defined as entry into all three arms on consecutive choices (the maximum number of alternations was the total number of entries minus 2). The percent alternation was calculated as (actual alternations/maximum alternations) x 100. The percent alternation was designated as the spontaneous alternation behavior of the mouse, was taken as a measure of memory performance.

**Thioflavin T binding assay**

The thioflavin T binding assay was performed by mixing aliquots of Aβ. Amyloid β-protein (human, 1–40), amyloid β-protein (human, 1–42), and amyloid β-protein (human, 1–43) were purchased from the Peptide Institute. We first examined aggregation property of individual Aβ40, Aβ42 and Aβ43 by incubating the peptide separately at 20 μM in 50 mM potassium phosphate buffer (PPB) (pH 7.4) at 37 ºC for 24 hrs with agitation. The stoichiometric effect of different Aβ species on aggregation was investigated in the mixture of Aβ40 and Aβ42 by adding and mixing Aβs in 50 mM PPB (pH 7.4) at molar concentrations of 20 μM : 2 μM : 0.2 μM (Aβ40 : Aβ42 : Aβ40/Aβ42/Aβ43 = 100 : 10 : 1) and incubating them at 37 ºC for 24 hrs with agitation. After incubation, thioflavin T was added to a final concentration of 5 μM, and thioflavin T fluorescence was measured at excitation and emission wavelengths of 442 nm and 485 nm were used, respectively.

**Neural cell toxicity assay**

Primary cortical neurons were isolated as previously described[23] and plated at a density of 5 x $10^4$ cells/well in 96 well plate ($n$ = 6 wells in each experimental conditions). Day in vitro (DIV) 10 to DIV14 cultures were treated with synthesized Aβ40, Aβ42 and Aβ43 peptide (Peptide Institute) at 0.1 to 10 μM of Aβs for 72 hr. These Aβ peptides were dissolved in 10% (v/v) of 60 mM NaOH and 90% (v/v) of 10 mM phosphate buffer, pH7.4, which was used as the vehicle[33]. SH-SY5Y cells were plated at a density of 2 x $10^4$ cells/well with 10% fetal bovine serum (FBS) supplemented medium in 96 well plate ($n$ = 6 wells in each experimental conditions), and incubated for 24 hr. Then, the media was replaced with media containing 1% of FBS, and treated with each Aβ peptides for 48 hr. Cell viability was determined using MTS assay (CellTiter96 Aqueous One Solution Cell Proliferation Assay Kit: Promega)[49], and LDH release as cell toxicity was performed using CytoTox-ONE Homogeneous Membrane Integrity Assay Kit (Promega)[33], according to the manufacturer's instructions and compared to vehicle treated cells, respectively.

**AD brain sections**

Postmortem AD brain tissues were kindly provided by J.Q. Trojanowski and V.M.-Y. Lee (University of Pennsylvania, Philadelphia, PA). The tissues had been fixed with ethanol or formalin and embedded in paraffin. This study was approved by the Institutional Review Board of the RIKEN Brain Science Institute.

**Reffernces**

1. Blennow, K. de Leon, M.J. & Zetterberg, H. Alzheimer's disease. *Lancet* **368**, 387–403 (2006).

2. Miravalle, L. *et al*. Amino-terminally truncated Aβ peptide species are the main component of cotton wool plaques. *Biochemistry* **44**, 10810–10821 (2005).

3. Van Vickle, G.D. *et al*. TgCRND8 amyloid precursor protein transgenic mice exhibit an altered γ-secretase processing and an aggressive, additive amyloid pathology subject to immunotherapeutic modulation. *Biochemistry* **46**, 10317–10327 (2007).

4. Iizuka, T. *et al*. Amyloid β-protein ending at Thr43 is a minor component of some diffuse plaques in the Alzheimer's disease brain, but is not found in cerebrovascular amyloid. *Brain Res.* **702**, 275–278 (1995).

5. Parvathy, S. *et al*. Correlation between Aβx–40-, Aβx–42-, and Aβx–43-containing amyloid plaques and cognitive decline. *Arch. Neurol.* **58**, 2025–2032 (2001).

6. Welander, H. *et al*. Aβ43 is more frequent than Aβ40 in amyloid plaque cores from Alzheimer disease brains. *J. Neurochem.* **110**, 697–706 (2009).

7. Keller, L. *et al.* The *PSEN1* I143T mutation in a Swedish family with Alzheimer's disease: clinical report and quantification of Aβ in different brain regions. *Euro. J. Hum. Gene.* **18**, 1202–1208 (2010).

8. Qi-Takahara, Y. *et al*. Longer forms of amyloid β protein: Implications for the mechanism of intramembrane cleavage by γ-secretase. *J. Neurosci.* **25**, 436–445 (2005).

9. Takami, M. *et al*. γ-Secretase: Successive tripeptide and tetrapeptide release from the transmembrane domain of β-carboxyl terminal fragment. *J. Neruosci.* **29**, 13042–13052 (2009).

10. Shimojo, M. *et al*. Enzymatic characteristics of I213T mutant Presenilin-1/γ-secretase in cell models and knock-in mouse brains: FAD-linked mutation impairs γ-site cleavage of APP-CTFβ. *J. Biol. Chem.* **283**, 16488–16496 (2008).

11. Jarrett, J.T. Berger, E.P. & Lansbury, P.T. Jr. The carboxy terminus of the β amyloid protein is critical for the seeding of amyloid formation: Implications for the pathogenesis of Alzheimer's disease. *Biochemistry* **32**, 4693–4697 (1993).

12. Bitan, G. *et al*. Amyloid β-protein (Aβ) assembly: Aβ40 and Aβ42 oligomerize through distinct pathways. *Proc. Natl. Acad. Sci. USA* **100**, 330–335 (2003).

13. Nakaya, Y. *et al*. Random mutagenesis of presenilin-1 identifies novel mutants exclusively generating long amyloid β-peptides. *J. Biol. Chem.* **280**, 19070–19077 (2005).

14. Godbolt, A.K. *et al*. A presenilin 1 R278I mutation presenting with language impairment. *Neurology* **63**, 1702–1704 (2004).

15. Shen, J. *et al*. Skeletal and CNS defects in Presenilin-1-deficient mice. *Cell* **89**, 629–639 (1997).

16. Wong, P.C. *et al*. Presenilin 1 is required for Notch1 and Dll1 expression in the paraxial mesoderm. *Nature* **387**, 288–292 (1997).

17. Culvenor, J.G. *et al*. Characterization of presenilin complexes from mouse and human brain using blue native gel electrophoresis reveals high expression in embryonic brain and minimal change in complex mobility with pathogenic presenilin mutations. *Eur. J. Biochem.* **271**, 375–385 (2003).

18. Evin, G. *et al*. Transition-state analogue γ-secretase inhibitors stabilize a 900 kDa presenilin/nicastrin complex. *Biochemistry* **44**, 4332–4341 (2005).

19. Thinakaran, G. *et al*. Endoproteolysis of presenilin 1 and accumulation of processed derivatives in vivo. *Neuron* **17**, 181–190 (1996).

20. Lee, M.K. *et al*. Hyperaccumulation of FAD-linked presenilin 1 variants in vivo. *Nature Med.* **3**, 756–760 (1997).

21. Kaneko, H. *et al*. Enhanced accumulation of phosphorylated α-synuclein and

elevated β-amyloid 42/40 ratio caused by expression of the presenilin-1 ΔT440 mutant associated with familial Lewy body disease and variant Alzheimer's disease. *J. Neurosci.* **27**, 13092–13097 (2007).

22. Schroeter, E.H. *et al.* A presenilin dimer at the core of the γ-secretase enzyme: Insight from parallel analysis of Notch1 and APP proteolysis. *Proc. Natl. Acad. Sci. USA* **100**, 13075–13080 (2003).

23. Hama, E. Shirotani, K. Iwata, N. & Saido, T.C. Effects of neprilysin chimeric proteins targeted to subcellular compartments on amyloid β peptide clearance in primary neurons. *J. Biol. Chem.* **279**, 30259–30264 (2004).

24. Kumar-Singh, S. *et al*. Mean age-of-onset of familial Alzheimer disease caused by presenilin mutations correlates with both increased Aβ42 and decreased Aβ40. *Human Mutation* **27**, 686–695 (2006).

25. Wang, R. Wang, B. He, W. & Zheng, H. Wild-type presenilin 1 protects against Alzheimer disease mutation-induced amyloid pathology. *J. Biol. Chem.* **281**, 15330–15336 (2006).

26. Maeda, J. *et al*. Longitudinal, quantitative assessment of amyloid, neuroinflammation, and anti-amyloid treatment in a living mouse model of Alzheimer's disease enabled by positron emission tomography. *J. Neurosci.* **27**, 10957–10968 (2007).

27. Saido, T.C. *et al*. Dominant and differential deposition of distinct β-amyloid peptide species, AβN3(pE), in senile plaques. *Neuron* **14**, 457–466 (1995).

28. Schilling, S. *et al*. Glutaminyl cyclase inhibition attenuates pyroglutamate Aβ and Alzheimer's disease-like pathology. *Nature Med.* **14**, 1106–1111 (2008).

29. Zhang, C. et al. Presenilins are essential for regulating neurotransmitter release. *Nature* **460,** 632–637 (2009).

30. Russo, C. *et al*. Presenilin-1 mutations in Alzheimer's disease. *Nature* **405**, 531–532 (2000).

31. McGowan, E. *et al*. Aβ42 is essential for parenchymal and vascular amyloid deposition in mice. *Neuron* **47**, 191–199 (2005).

32. Kim, J. *et al*. Aβ40 inhibits amyloid deposition in vivo. *J. Neurosci.* **27**, 627–633 (2007).

33. Ono, K., Condron, M. and Teplow, D.B. Effects of the English (H6R) and Tottori (D7N) familial Alzheimer disease mutations on amyloid β-protein assembly and toxicity. *J. Biol. Chem.* **285**, 23186–23197 (2010).

34. Jan, A. *et al.* The ratio of monomeric to aggregated forms of Aβ40 and Aβ42 is an important determinant of amyloid-β aggregation, fibrillogenesis, and toxicity. *J. Biol. Chem.* **283**, 28176–28189 (2008).

35. Huppert, S. *et al*. Embryonic lethality in mice homozygous for a processing-deficient allele of Notch1. *Nature* **405**, 966–970 (2000).

36. Ikeuchi, T. *et al*. Familial Alzheimer disease-linked presenilin 1 variants enhance production of both Aβ1–40 and Aβ1–42 peptides that are only partially sensitive to a potent aspartyl protease transition state inhibitor of "γ-secretase". *J. Biol. Chem.* **278**, 7010–7018 (2003).

37. Serneels, L. *et al*. γ-Secretase heterogeneity in the Aph1 subunit: Relevance for Alzheimer's disease. *Science* **324**, 639–642 (2009).

38. Bentahir, M. *et al*. Presenilin clinical mutations can affect γ-secretase activity by different mechanisms. *J. Neruochem.* **96**, 732–742 (2006).

39. Deng, Y. *et al.* Deletion of presenilin 1 hydrophilic loop sequence leads to imparired γ-secretase activity and exacerbated amyloid pathology. *J. Neurosci.* **26**, 3845–3854 (2006).

40. Hara, H. *et al*. Development of a safe oral Aβ vaccine using recombinant adeno-associated virus vector for Alzheimer's disease. *J. Alz. Dis.* **6**, 483–488 (2004).

41. Mouri A. *et al*. Oral vaccination with a viral vector containing Aβ cDNA attenuates age-related Aβ accumulation and memory deficits without causing inflammation in a mouse Alzheimer model. *FASEB J*. **21**, 2135–2148 (2007).

42. Kimura, N. *et al*. Senile plaques in an aged Western Lowland Gorilla. *Exp. Anim.* **50**, 77–81 (2001).

43. Sturchler-Pierrat, C. *et al*. Two amyloid precursor protein transgenic mouse models with Alzheimer disease-like pathology. *Proc. Natl. Acad. Sci. USA* **94**, 13287–13292 (1997).

44. Huang, S.-M. *et al*. Neprilysin-sensitive synapse-associated amyloid-β peptide oligomers impair neuronal plasticity and cognitive function. *J. Biol. Chem.* **281**, 17941–17951 (2006).

45. Kopan, R. Schroeter, E.H. Weintraub, H. & Nye, J.S. Signal transduction by activated mNotch: Importance of proteolytic processing and its regulation by the extracellular domain. *Proc. Natl. Acad. Sci. USA* **93**, 1683–1688 (1996).

46. Iwata, N. *et al*. Presynaptic localization of neprilysin contributes to efficient clearance of amyloid-β peptide in mouse brain. *J. Neurosci.* **24**, 991–998 (2004).

47. Iwatsubo, T. *et al.* Visualization of Aβ42(43) and Aβ40 in senile plaques with end-specific Aβ monoclonals: Evidence that an initially deposited species is Aβ42(43). *Neuron* **13**, 45–53 (1994).

48. Enya, M. *et al*. Appearance of sodium dodecylsulfate-stable amyloid β-protein (Aβ) dimer in the cortex during aging. *Am. J. Pathol.* **154**, 271–279 (1999).

49. Ryan, D.A. *et al.* An improved method for generating consistent soluble amyloid-beta oligomer preparations for *in vitro* neurotoxicity studies. *J. Neurosci. Res.* **190**, 171–179 (2010).

50. Arango, D. *et al.* Systemic genetic study of Alzheimer disease in Latin America: Mutation frequencies of the amyloid β precursor protein and presenilin gene in Colombia. *Am. J. Med. Genet.* **103**, 138–143 (2001).

Saido T.C.: Fig. 1

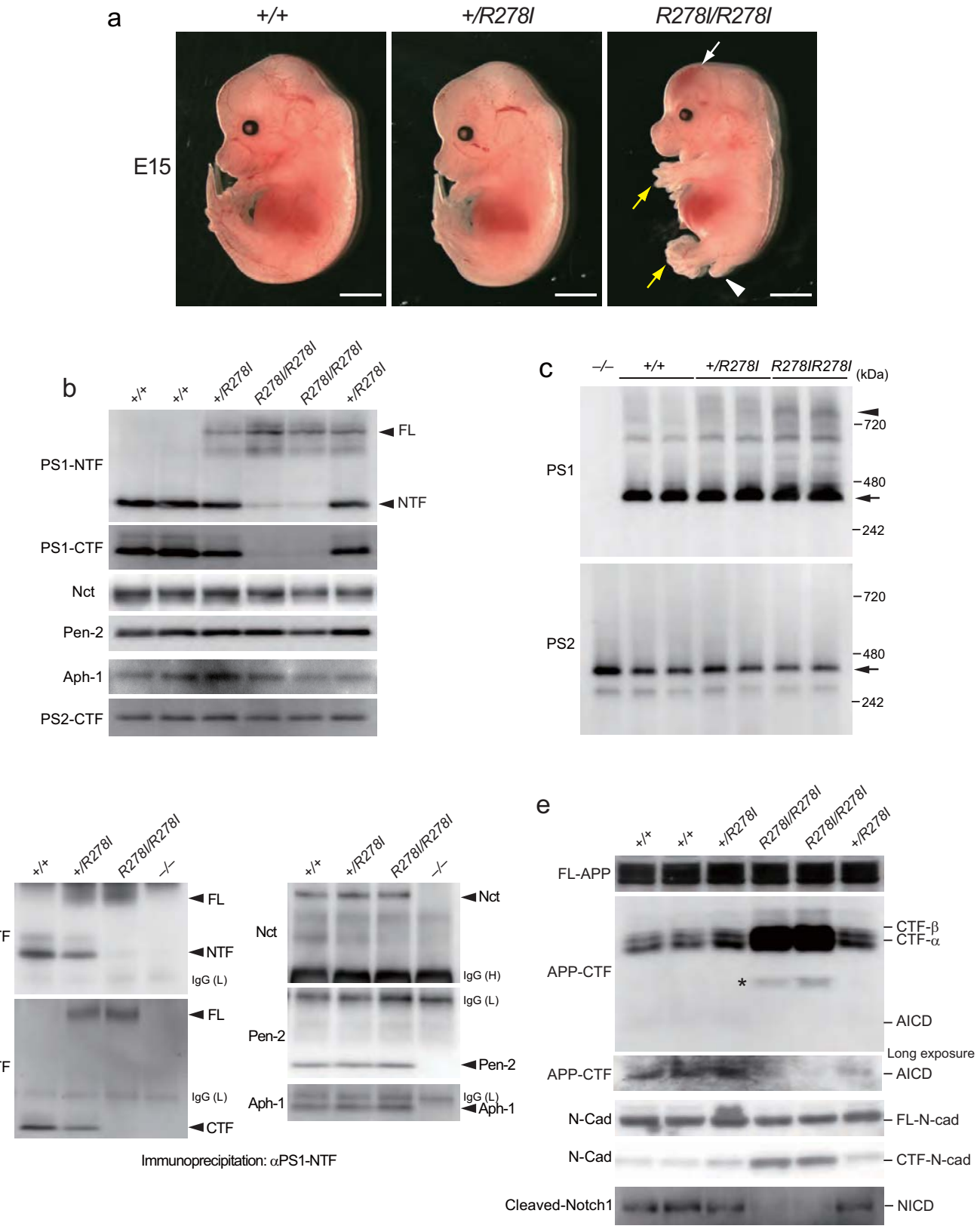

Saido T.C.: Fig. 2

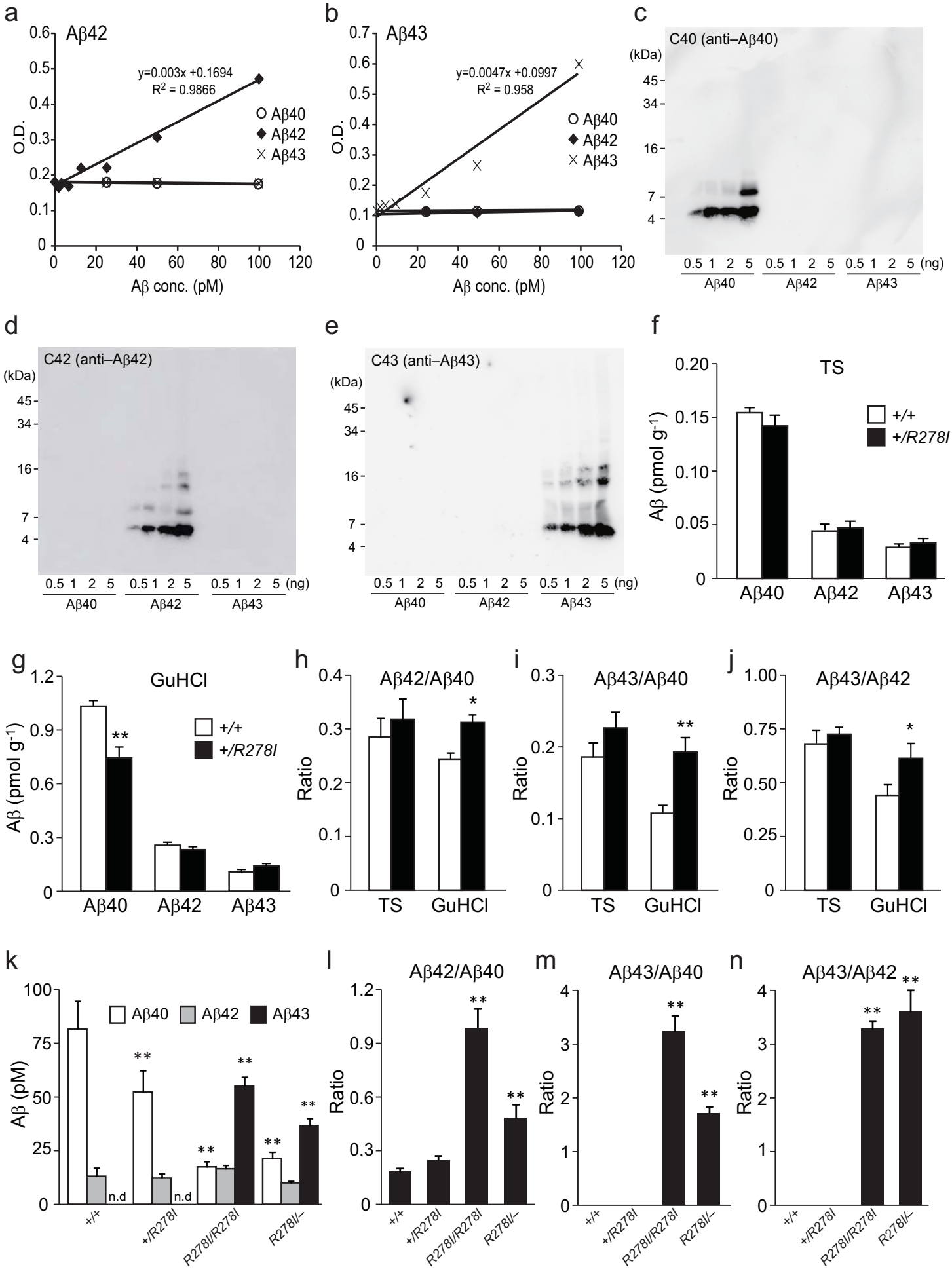

Fig. 3

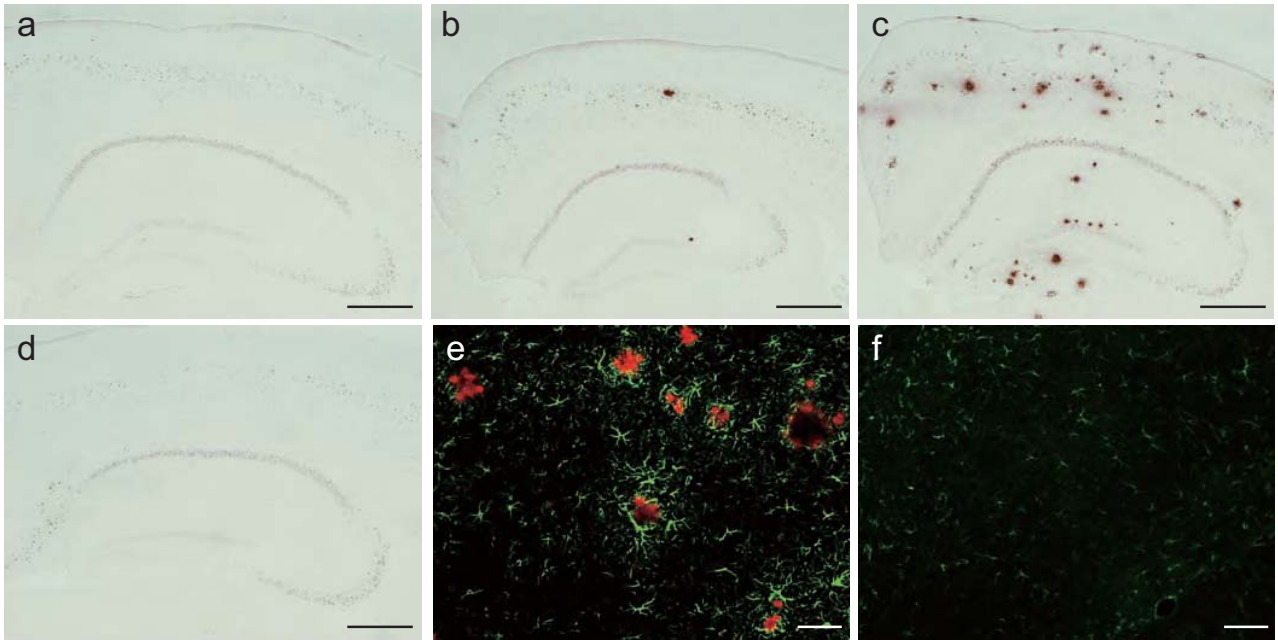
a
b
c
d
e
f

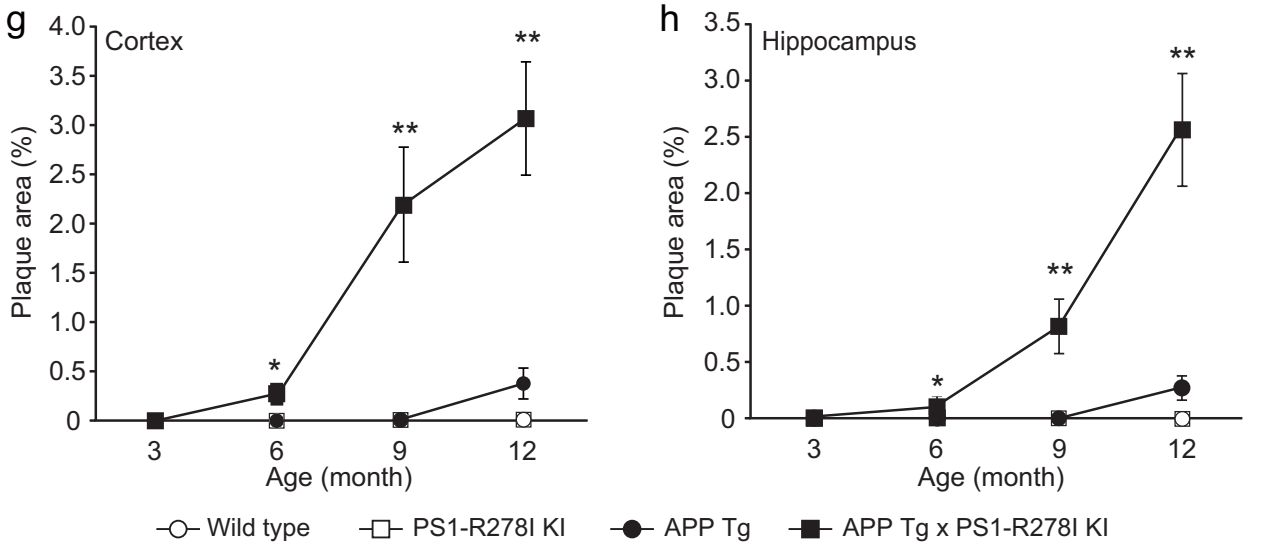
g
Cortex
Plaque area (%)
Age (month)
h
Hippocampus
Plaque area (%)
Age (month)
Wild type
PS1-R278I KI
APP Tg
APP Tg x PS1-R278I KI

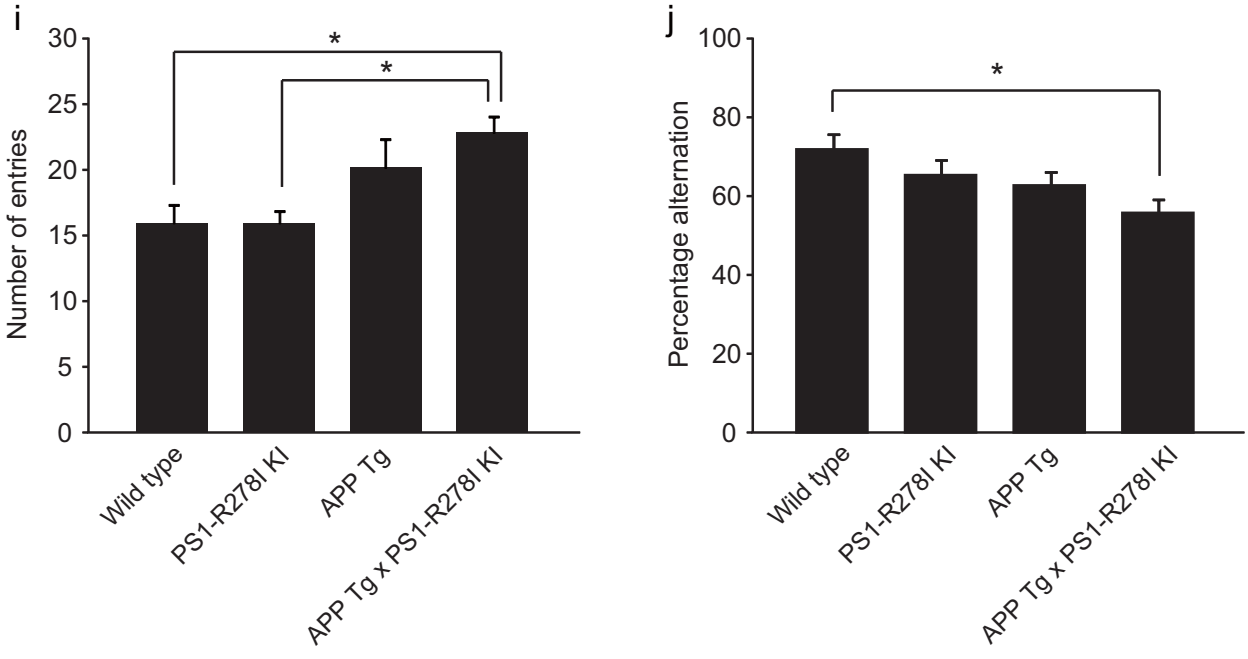
i
Number of entries
Wild type
PS1-R278I KI
APP Tg
APP Tg x PS1-R278I KI
j
Percentage alternation
Wild type
PS1-R278I KI
APP Tg
APP Tg x PS1-R278I KI

Saido T.C.: Fig. 4

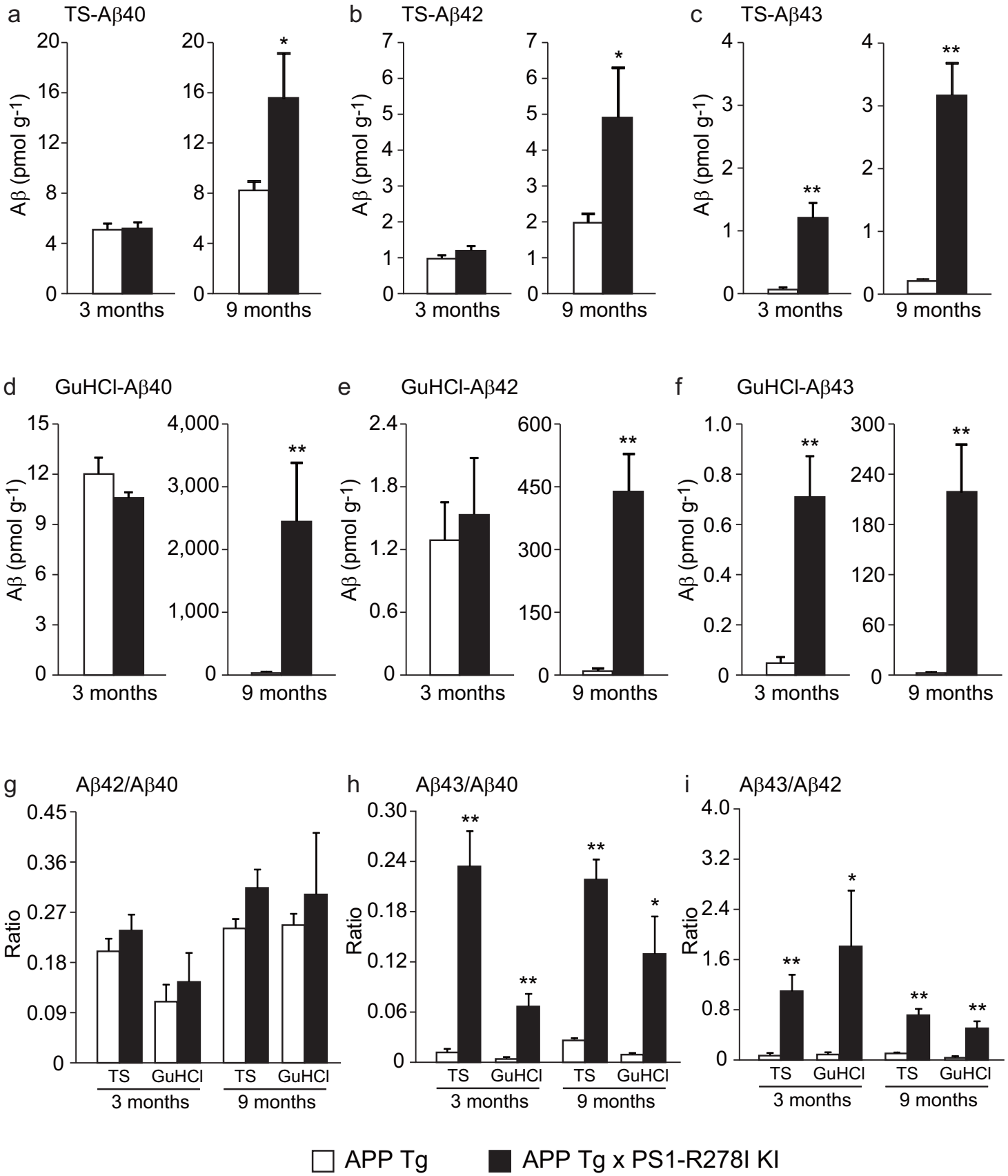

Saido T.C.: Fig. 5

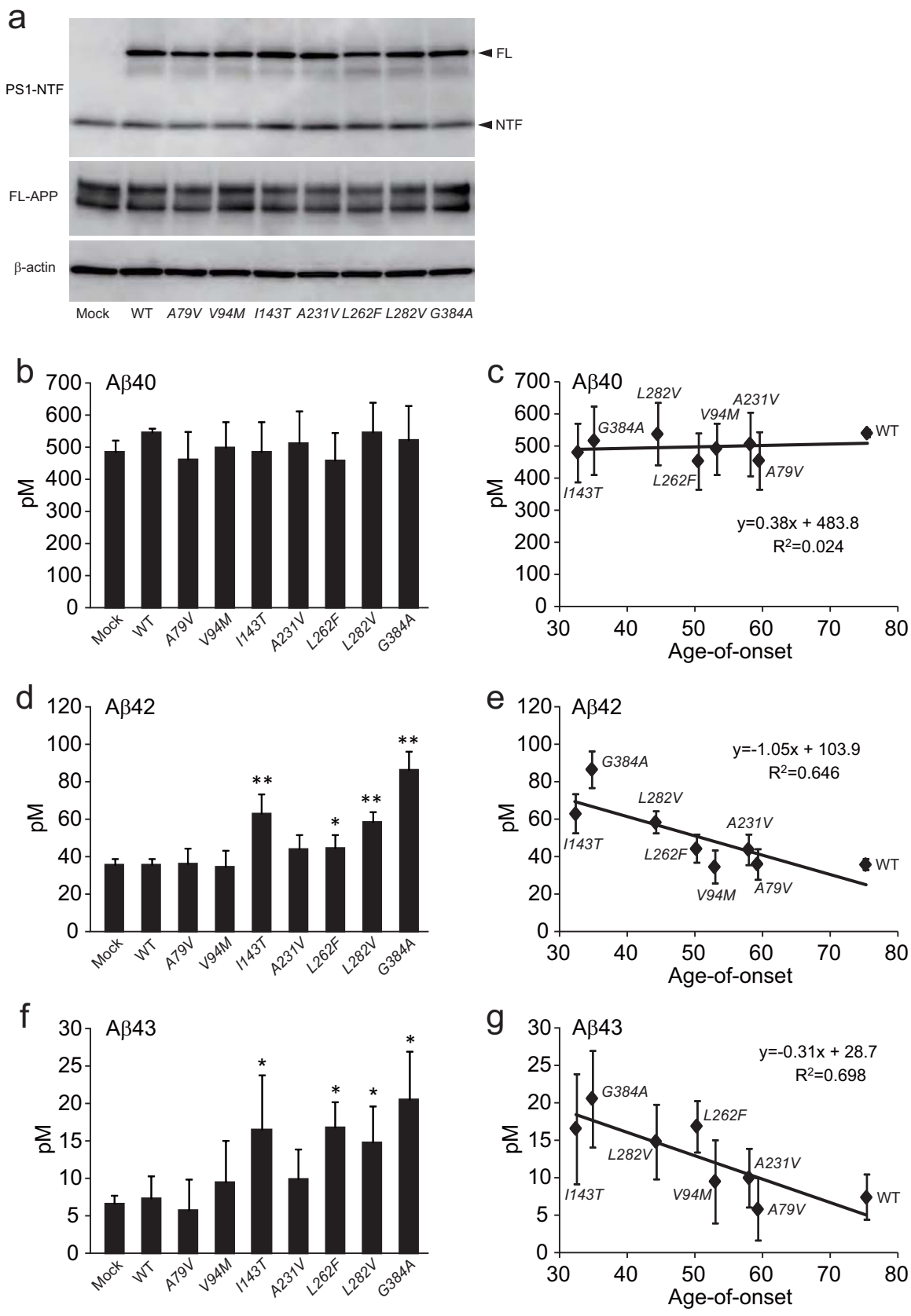

Saido T.C.: Fig. 6

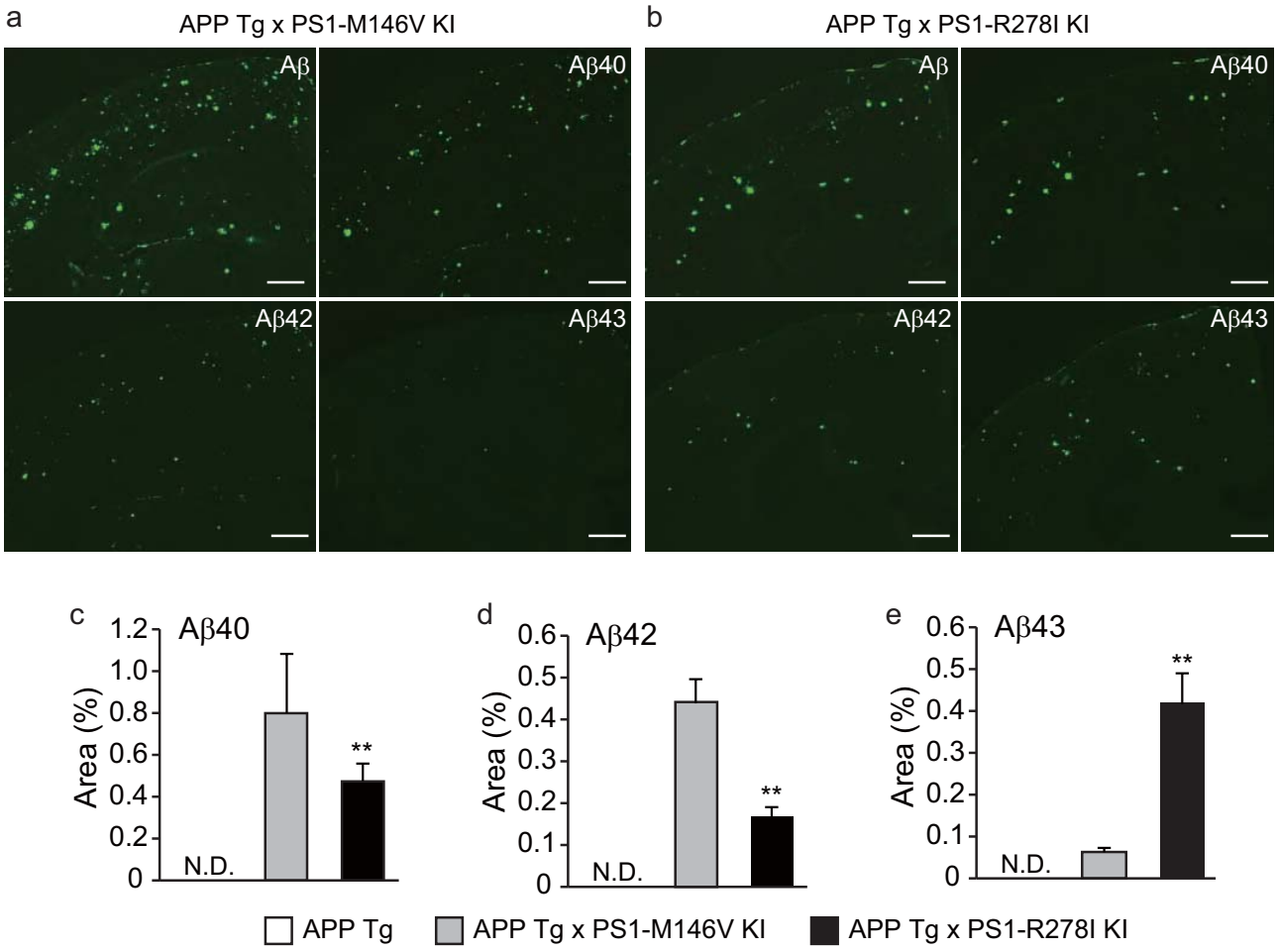


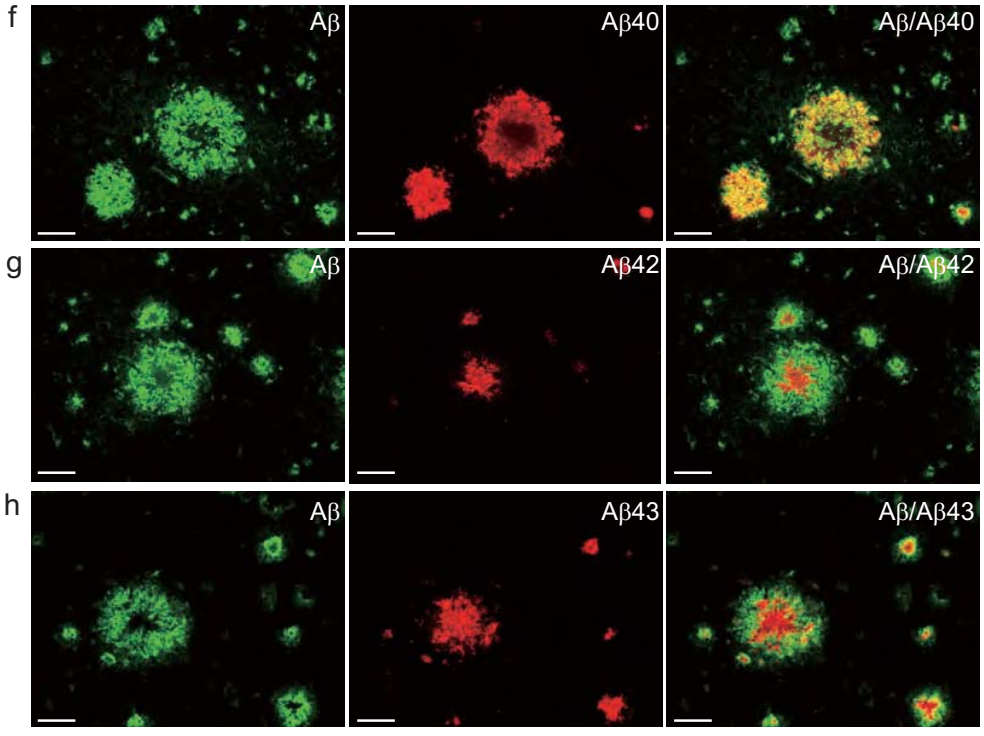

Saido T.C.: Fig. 7

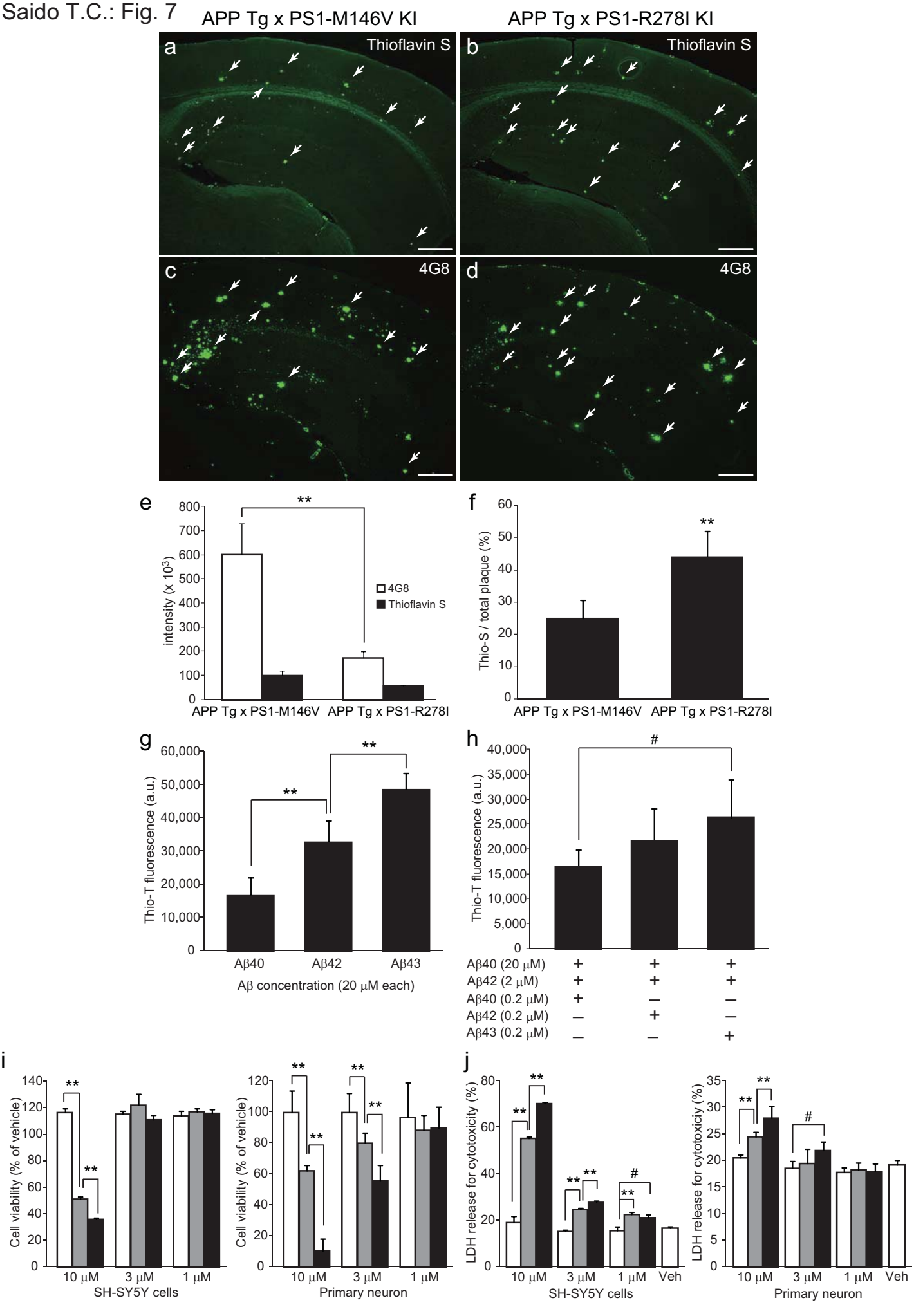

Saido T.C.: Fig. 8